

Boosting Determinant Quantum Monte Carlo with Submatrix Updates: Unveiling the Phase Diagram of the 3D Hubbard Model

Fanjie Sun¹ and Xiao Yan Xu^{1, 2, *}

¹*Key Laboratory of Artificial Structures and Quantum Control (Ministry of Education),
School of Physics and Astronomy, Shanghai Jiao Tong University, Shanghai 200240, China*

²*Hefei National Laboratory, Hefei 230088, China*

(Dated: April 16, 2024)

The study of strongly correlated fermionic systems, crucial for understanding condensed matter physics, has been significantly advanced by numerical computational methods. Among these, the Determinant Quantum Monte Carlo (DQMC) method stands out for its ability to provide exact numerical solutions. However, the computational complexity of DQMC, particularly in dealing with large system sizes and the notorious sign problem, limits its applicability. We introduce an innovative approach to enhance DQMC efficiency through the implementation of submatrix updates. Building upon the foundational work of conventional fast updates and delay updates, our method leverages a generalized submatrix update algorithm to address challenges in simulating strongly correlated fermionic systems with both onsite and extended interactions at both finite and zero temperatures. We demonstrate the method's superiority by comparing it with previous update methods in terms of computational complexity and efficiency. Specifically, our submatrix update method significantly reduces the computational overhead, enabling the simulation of system sizes up to 8,000 sites without pushing hard. This advancement allows for a more accurate determination of the finite temperature phase diagram of the 3D Hubbard model at half-filling. Our findings not only shed light on the phase transitions within these complex systems but also pave the way for more effective simulations of strongly correlated electrons, potentially guiding experimental efforts in cold atom simulations of the 3D Hubbard model.

I. INTRODUCTION

In recent years, theoretical research on strongly correlated fermionic systems has become a focal point in the field of condensed matter physics. With the proposal of various approximate models for such systems and the flourishing development of computer technology, numerical computational methods have garnered increasing attention in this domain. Among various numerical methods, the exact diagonalization (ED) method [1] stands out as a universal approach capable of accurately determining system properties. However, its computational complexity exhibits an exponential increase with the size of the system, posing a significant challenge for precise treatment of large systems. The density matrix renormalization group (DMRG) method [2, 3] demonstrates accurate solutions for one-dimensional systems, but it requires exponentially large bond dimensions due to the area law or even faster increasing of entanglement for higher dimensional systems. The tensor network (TN) method, which naturally reflects the entanglement structure has been achieving promising progress, but its computational complexity is still a very high power of bond dimensions. The dynamical mean field theory (DMFT) [4] excels in combining with LDA for material calculations, but inherently loses long-range spatial fluctuations, and may encounter challenges in converging to physically meaningful solutions under strong correlation conditions [5, 6], thereby compromising computational

accuracy. The quantum Monte Carlo (QMC) method stands out as a numerically exact method, however, it usually suffers from the sign problem.

For models free from the sign problem, the QMC method is expected to accurately simulate very large system sizes. This is indeed the case for quantum spin systems, for example, Stochastic Series Expansion (SSE)-QMC method can typically handle hundreds of thousands of sites. However, for fermionic systems, the simulation becomes much heavier. For example, determinant QMC (DQMC) [13–21], which is usually also called Blankenbecler-Scalapino-Sugar (BSS) method [13] or auxiliary field QMC (AFQMC), has found widespread application in solving strongly correlated fermionic systems, yielding numerous meaningful scientific results [22–49]. Despite its significant success, the DQMC algorithm still faces substantial limitations. Due to the tedious processing of a large number of Green's function matrices, including updates and matrix multiplications during the simulation, the DQMC algorithm exhibits high computational complexity $\mathcal{O}(\beta N^3)$, where N is the total number of lattice sites, β is the inverse temperature. This complexity and its huge prefactor together make it challenging to simulate very large system size, thus usually one cannot faithfully extrapolate the limited finite size results to the thermodynamic limit and obtain accurate phase transition properties. For instance, in the simulation of interacting Dirac fermion systems with Gross-Neveu transition, the critical exponents do not converge among different simulations on the same universality class [30, 35, 50]. Among those simulations, the typical system size is around 1000 sites, and only a few

* xiaoyanxu@sjtu.edu.cn

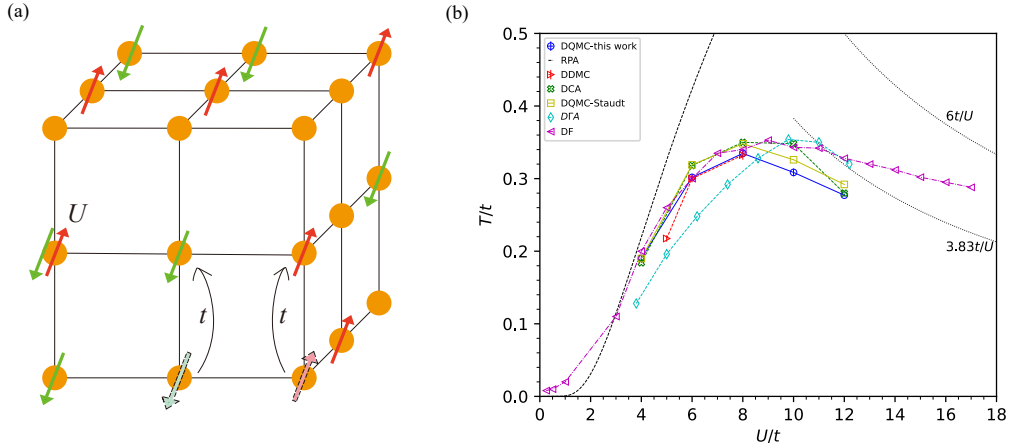


FIG. 1. (a) The Hubbard model on a three-dimensional cubic lattice. The parameter t describes the hopping of electrons between nearest neighbor (NN) sites i and j , while U represents the amplitude of the onsite Hubbard repulsive interaction. (b) The phase diagram of the Néel transition for the three-dimensional half-filled Hubbard model on a cubic lattice, as obtained by DQMC in this work (blue circles). The comparison curves are obtained by the random phase approximation (RPA) from Refs. [7] (dashed black line), determinantal diagrammatic Monte Carlo (DDMC; red right triangles) [8], dynamical cluster approximation (DCA; green X-shaped) [9], DQMC-Staudt's work (DQMC; yellow square) [10], dynamical vertex approximation (DVA; light blue rhombus) [11], the dual-fermion multiscale approach (DF; purple left triangles) [12].

examples approach about 2500 sites [35]. Another example is the three-dimensional half-filled Hubbard model, current applications of the DQMC algorithm are limited to systems with only around 1000 lattice sites [10]. This limitation poses challenges in accurately determining the temperature for the Néel antiferromagnetic phase transition. Therefore, increasing the efficiency of simulating fermionic systems is an urgent task. One promising direction relies on the developing Hamiltonian lattice field theories [51], with a large finite temporal lattice spacing, a simulation of 10,000 sites is achieved, and a simulation of 4,096 sites in the small temporal lattice spacing limit is obtained. Another attempt comes from using hybrid Monte Carlo (HMC) to study strongly correlated fermionic systems [52], which is expected to have lower computational complexity, but it turns out there are ergodicity issues due to zeros of the determinant in models such as Hubbard model. Algorithms designed to avoid these ergodicity issues may introduce high computational complexity [52] or explicitly symmetry breaking [50, 53–56]. For the long range coulomb coupling problem, when the fermion determinant is not too ill-conditioned, HMC can simulate amazing large system size with more than 20,000 lattice sites [57]. There is also encouraging progress in developing fermionic numerical methods without determinants [58], but their computational efficiency for large systems is still waiting to be tested.

Directly improving the efficiency of DQMC has always been a challenging problem. Based on self-learning Monte Carlo method [59, 60], it is able to improve the simulation system size up to 10,000 sites at very high temperature for a spin-fermion model, but the speedup

strongly depends on the accuracy of the effective model, which is used to guide the update. Low-rank approximation also shows significant speedup for the low density case [61], however, its theoretical accuracy for large densities is not well established theoretically. Recently, we proposed a generalized delay update algorithm [62], originally proposed in Refs. [63, 64] to study onsite Hubbard models at finite temperatures in Hirsh-Fye QMC and continuous-time QMC. We apply it in DQMC and have generalized it to study models with extended interactions at both finite and zero temperatures. Furthermore, there is still room left to improve the efficiency further by using the submatrix update [64], which has already been implemented in Hirsh-Fye QMC and continuous-time QMC [64, 65]. In this article, we implement the submatrix update in DQMC, and generalize it to handle extended interactions as well as zero-temperature cases. With the help of the speedup gain from submatrix update, we are able to simulate system sizes up to 8,000 sites without pushing hard, thus being able to accurately determine the finite temperature phase diagram of the 3D Hubbard model at half-filling, as shown in Fig. 1. We anticipate this more accurate phase diagram will help to guide the cold atom simulation of the 3D Hubbard model [66].

In the following, we briefly compare three different update schemes used in DQMC, the conventional fast update, the delay update, and the submatrix update. In the DQMC algorithm, Trotter decomposition is employed to partition the inverse temperature β into numerous small slices ($\beta = L_\tau \Delta_\tau$), while the Hubbard-Stratonovich (HS) transformation is utilized to decouple the interaction term by introducing auxiliary fields. Typically, there

are $\mathcal{O}(\beta N)$ auxiliary fields (where N represents the system size). We assume each auxiliary field connects k spatial sites, and consider only when k does not scale with system size, namely, we only consider interactions with locality. After those steps, the problem has been transformed to be a problem with fermion bilinears coupled to auxiliary fields, such that the fermion degrees of freedom can be exactly traced out, resulting in a determinant of the inverse of the equal-time Green's function matrix as the Boltzmann weight for each configuration of auxiliary fields. If any Boltzmann weight is semi-positive, which means there is no sign problem, we can interpret it as probability, such that Monte Carlo can be used to perform importance sampling. If there is a sign problem, we usually need to define a sign free referenced system to perform the Monte Carlo simulation. In this case, the average sign usually shows an exponentially decay with system size, resulting in an exponentially scaling of complexity to achieve a controllable error bar. Of course, there are exceptions. It was first observed in a simulation that the average sign could algebraically decay with system size [67]. This phenomenon was later also found in several other cases [68]. Interested readers can refer to Refs. [67–69] for more details. Here, let's focus on cases free from the sign problem and note that all the update schemes discussed here also apply to cases with a sign problem.

During the simulation, we try to flip auxiliary fields one by one by performing local updates. We define *a sweep* as traversing auxiliary fields across all spatio-temporal sites in a sequence that starts from an initial site, progresses to the final site, and then reverses back to the initial site. In the following, when we talk about the computation complexity, by default we talk about the complexity per sweep. When flipping an auxiliary field at a specific spatio-temporal site, the proposed flip alters only a small region of the coefficient matrices for fermion bilinears. Consequently, the new Green's function matrix differs from the old one by a low-rank (rank k) matrix. Therefore, the calculation of the ratio of the determinant can be simplified by using Sylvester's determinant theorem, resulting only $\mathcal{O}(k^3)$ complexity to calculate the determinant ratio. If the proposed flip is accepted, we update the full Green's function by using the fact that the new one and the old one only differ by a low rank (rank k) matrix. In the code, this can be done by Level 1 BLAS. This is so called *fast update*. The fast update scheme can be further improved by using delay update. The update of full Green's function can be delayed as the calculation of the determinant ratio only requires a small part of the Green's function, therefore we can store the intermediate vectors which will be used to calculate the determinant ratio for each local update, and finally be used to update the full Green's function after n_d number of vectors are accumulated, where n_d is determined by test in practice, and a suggested value is presented in the detailed discussion of the algorithm in the following. The final update of the full Green's function is done

by Level 3 BLAS. This is the basic idea of *delay update*, and it makes better usage of cache by replace Level 1 BLAS with Level 3 BLAS, which accelerates the calculation. However, using intermediate vectors to calculate determinant ratios will bring additional overhead, which has complexity $\mathcal{O}(\beta n_d N^2)$ per sweep. As this additional overhead is implemented with Level 1 BLAS, its time cost can surpass the time cost for the update of Green's function in practical calculation if one increase n_d , as shown in Fig. 4. The submatrix update can reduce this part to be $\mathcal{O}(\beta n_d^2 N)$, thus significantly reduce the computation with Level 1 BLAS. The computation complexity for all update scheme are summarized in Table I.

TABLE I. The computational complexity and types of computations required for various local updates. Here, 'intermediate overheads' refer to the calculations needed to obtain intermediate matrices/vectors for calculating the determinant ratio or to accumulate vectors used to finally update the Green's function, and 'update-G' refers to the calculations for updating the entire Green's function. 'Level 1' means Level 1 BLAS, and 'Level 3' means Level 3 BLAS. See Sec. II for more details.

	fast update	delay update	submatrix update
Intermediate overheads	-	$\mathcal{O}(\beta n_d N^2)$	$\mathcal{O}(\beta n_d^2 N)$
		Level 1	Level 1
update-G	$\mathcal{O}(\beta N^3)$	$\mathcal{O}(\beta N^3)$	$\mathcal{O}(\beta N^3 + \beta n_d N^2)$
	Level 1	Level 3	Level 3

The remaining part of the article is structured as follows: In Section II, we introduce the basic formalism of the submatrix update method. In Section III, we compare the efficiency of the submatrix update method with the delay update method proposed previously [62]. This comparison is conducted on both the Hubbard model and the spinless t - V model on a two-dimensional square lattice. Additionally, we provide the phase diagram for the antiferromagnetic Néel order phase transition in the three-dimensional Hubbard half-filled model on a cubic lattice. Finally, we present a brief conclusion and discussion in Section IV.

II. METHOD

We first revisit the key aspects of the derivation presented in Ref. [62] within the framework of the fast update and the delay update. Then we introduce the submatrix updates for DQMC, outlining the notation and conventions. We focus on the finite temperature version of DQMC (DQMC-finite-T) and address the zero-temperature case in Appendix D. Our discussion is limited to models without sign problems, achieved through appropriate HS transformations. Taking the Hubbard model [70–73] as an example, with Hamiltonian

$$H_{tU} = H_0 + H_U \quad (1)$$

where $H_0 = -t \sum_{\langle i,j \rangle, \alpha} (c_{i,\alpha}^\dagger c_{j,\alpha} + \text{H.c.})$ and $H_U = \frac{U}{2} \sum_i (n_i - 1)^2$. Here, $c_{i,\alpha}^\dagger$ represents an electron creation operator on site i , where $\alpha = \uparrow / \downarrow$ denotes the spin polarization direction of electrons, and $n_i = \sum_\alpha c_{i\alpha}^\dagger c_{i\alpha}$ represents the electron occupation. The term H_0 describes the hopping of electrons between nearest neighbor (NN) sites i and j , while H_U accounts for the onsite Coulomb repulsion between two electrons.

The Hubbard model effectively captures the competitive relationship between the kinetic energy term associated with electron hopping and the potential energy term arising from Coulomb repulsion. In this study, we employ the following Hubbard-Stratonovich (HS) transformation to decouple the interaction term into a coupling between fermions and bosonic auxiliary fields.

$$e^{-\Delta_\tau \frac{U}{2} \sum_i (n_i - 1)^2} = \frac{1}{4} \sum_{s=\pm 1, \pm 2} \gamma(s) e^{i\alpha_U \sum_i \eta(s) (n_i - 1)} + O(\Delta_\tau^4) \quad (2)$$

In the HS transformation, s represents an auxiliary field, $\alpha_U = \sqrt{\Delta_\tau U}$, and $\gamma(\pm 1) = 1 + \frac{\sqrt{6}}{3}$, $\gamma(\pm 2) = 1 - \frac{\sqrt{6}}{3}$, $\eta(\pm 1) = \pm \sqrt{2(3 - \sqrt{6})}$, $\eta(\pm 2) = \pm \sqrt{2(3 + \sqrt{6})}$. By tracing out the degrees of freedom of the fermion, the partition function can be expressed as follows:

$$Z = \sum_s w_b[s] w_f[s] \quad (3)$$

For convenience, let's denote all auxiliary fields in all the spatial-time sites as \mathbf{s} . The bosonic weight can be clearly defined as

$$w_b[\mathbf{s}] \equiv \prod_{s \in \mathbf{s}} \frac{1}{4} \gamma(s) e^{-i\alpha_U \eta(s)}. \quad (4)$$

And the fermion weight can be expressed in the form of a determinant

$$w_f[\mathbf{s}] = \det [I + B_{\mathbf{s}}(\beta, 0)]. \quad (5)$$

$B_{\mathbf{s}}(\beta, 0)$ is the time evolution matrix from imaginary time 0 to imaginary time β . A general time evolution matrix from imaginary time $\tau_1 = l_1 \Delta_\tau$ to imaginary time $\tau_2 = l_2 \Delta_\tau$ ($\tau_2 \geq \tau_1$) is defined as

$$B_{\mathbf{s}}(\tau_2, \tau_1) = B_{\mathbf{s}}^{l_2} B_{\mathbf{s}}^{l_2-1} \cdots B_{\mathbf{s}}^{l_1+1} \quad (6)$$

where $B_{\mathbf{s}}^l = e^{V(\mathbf{s})} e^{-\Delta_\tau K}$ is the time evolution matrix for time slice l , where K is the coefficient matrix of the fermion bilinear of the non-interacting part $H_0 = \sum_{j,k} c_j^\dagger K_{j,k} c_k = \mathbf{c}^\dagger K \mathbf{c}$, and $V(\mathbf{s})$ is the coefficient matrix of the fermion bilinear after HS transformation of the interacting part $i\alpha_U \sum_i \eta(\mathbf{s}) n_i = \sum_{j,k} c_j^\dagger V(\mathbf{s})_{j,k} c_k = \mathbf{c}^\dagger V(\mathbf{s}) \mathbf{c}$. Note we have omitted the spin index, as it can be absorbed into the site index. For the case like Hubbard model where both K and $V(\mathbf{s})$ are block diagonal in

spin space, one can split the determinant in Eq. (5) into a product of two determinants for each spin, such that the determinant ratio can be calculated separately for each spin. However, to maintain generality, we discuss a general case in what follows.

A. Fast update

Let's now consider the local update of the auxiliary field \mathbf{s} . For a proposed update of auxiliary field at lattice site i and imaginary time slice l , $\mathbf{s}_{i,l} \rightarrow \mathbf{s}'_{i,l}$, it leads to a change $e^{V(\mathbf{s})} \rightarrow e^{V(\mathbf{s}')} = (I + \Delta)e^{V(\mathbf{s})}$, so the change Δ can be expressed as $\Delta = e^{V(\mathbf{s}')} e^{-V(\mathbf{s})} - I$, where \mathbf{s}' represents the proposed updated auxiliary fields. Then we calculate the acceptance ratio to determine whether to accept the proposed update. The determinant part ratio can be calculated in the following way.

$$\frac{w_f[\mathbf{s}']}{w_f[\mathbf{s}]} = \det [I + \Delta(I - G(\tau, \tau))] \quad (7)$$

where $G(\tau, \tau)$ is the equal-time Green's function matrix, defined as $G_{ij}(\tau, \tau) \equiv \langle c_i(\tau) c_j^\dagger(\tau) \rangle$, and is related to the time evolution matrix [13–21],

$$G(\tau, \tau) = (I + B(\tau, 0)B(\beta, \tau))^{-1} \quad (8)$$

Note that we have omitted the auxiliary field labels \mathbf{s} in the time evolution matrix B and the Green's function G , and will continue to use this notation by default. Generally, one can utilize unitary transformations to convert Δ into a sparse matrix with k non-zero diagonal elements. The unitary transformations can be absorbed into the time evolution matrix $B(\tau, 0)$ and $B(\beta, \tau)$. Let's assume that Δ is already transformed into its diagonal form and the positions of its k non-zero diagonal elements are x_1, x_2, \dots, x_k . Finally, we can apply Sylvester's determinant theorem to simplify the acceptance ratio to:

$$\frac{w_f[\mathbf{s}']}{w_f[\mathbf{s}]} = \det [S] \quad (9)$$

where

$$S = I_{k \times k} + \mathcal{V}D \quad (10)$$

is only a k -dimensional matrix, as well as $I_{k \times k}$, \mathcal{V} and D . $I_{k \times k}$ is an identity matrix, and \mathcal{V} and D are defined as

$$\mathcal{V} = \begin{bmatrix} -(G_{x_1 x_1} - 1) & -G_{x_1 x_2} & \cdots \\ -G_{x_2 x_1} & -(G_{x_2 x_2} - 1) & \cdots \\ \vdots & \vdots & \ddots \end{bmatrix}_{k \times k} \quad (11)$$

$$D = \begin{bmatrix} \Delta_{x_1 x_1} & & \\ & \Delta_{x_2 x_2} & \\ & & \ddots \end{bmatrix}_{k \times k} \quad (12)$$

Once the proposed update is accepted, in the fast update scheme, one utilizes the Woodbury matrix identity to update the entire Green's function matrix. The Green's function matrices before (denoted as G) and after (denoted as G') the update only differ by a rank- k matrix which can be represented as a product of three matrices: $\mathbb{U}\mathbb{S}\mathbb{V}$,

$$G' = G + \mathbb{U}\mathbb{S}\mathbb{V} \quad (13)$$

where the matrix \mathbb{U} , \mathbb{S} and \mathbb{V} have dimensions $N \times k$, $k \times k$ and $k \times N$ respectively, and have the following form:

$$\mathbb{U} = [G_{:,x_1} | G_{:,x_2} | \cdots]_{N \times k} \quad (14)$$

$$\mathbb{S} = DS^{-1} \quad (15)$$

$$\mathbb{V} = \left([G_{x_1,:} - e_{x_1} | G_{x_2,:} - e_{x_2} | \cdots]^T \right)_{k \times N} \quad (16)$$

where e_{x_j} denotes a length- N row vector with 'one' at position x_j and zero at all other positions, $G_{:,x_j}$ denotes column x_j of G , and $G_{x_j,:}$ denotes row x_j of G . This concludes the basic formulation for the fast update method.

B. Delay update

For the delay update, we follow Ref. [62] and review the key steps. The delay update basically delays the entire Green's function matrix update. We store the intermediate \mathbb{U} , \mathbb{S} and \mathbb{V} matrices, and for any intermediate step i , the Green's function can be calculated with the following form

$$G^{(i)} = G^{(0)} + \sum_{m=1}^i \mathbb{U}^{(m)} \mathbb{S}^{(m)} \mathbb{V}^{(m)}. \quad (17)$$

However, in practice, we do not calculate the entire Green's function at every step i . Instead, we only calculate a small region of $G^{(i)}$ necessary for calculating the determinant ratio and the intermediate \mathbb{U} , \mathbb{S} , and \mathbb{V} matrices. Finally, we calculate the entire Green's function matrix when $i = n_d$, with n_d in principle depending on the computation platform. Based on our test over several different platforms [62], setting $kn_d = 2^\lambda$, where $\lambda = \min[6, \lceil \log_2 \frac{N}{20} \rceil]$, is a good choice.

C. Submatrix update

The submatrix update can further improve the efficiency [63, 64]. To facilitate the derivation of the submatrix update method, we rewrite the i -th update of the Green's function in the fast update method as equations (13) as follows:

$$G^{(i)} = G^{(i-1)} + \mathbb{U}^{(i)} \mathbb{S}^{(i)} \mathbb{V}^{(i)} \quad (18)$$

$$\mathbb{S}^{(i)} = D^{(i)} (I_{k \times k} + \mathcal{V}^{(i)} D^{(i)})^{-1} \quad (19)$$

For convenience, we use the inverse of the Green's function matrix, defined as:

$$A^{(i)} \equiv (G^{(i)})^{-1} \quad (20)$$

Using the Woodbury matrix identity, the Eq. (18) can be rewritten as

$$\begin{aligned} A^{(i)} &= A^{(i-1)} - P_{N \times k} \left[x^{(i)} \right] D^{(i)} P_{k \times N} \left[x^{(i)} \right] \\ &\quad + P_{N \times k} \left[x^{(i)} \right] D^{(i)} P_{k \times N} \left[x^{(i)} \right] A^{(i-1)} \\ &= \left[I + P_{N \times k} \left[x^{(i)} \right] D^{(i)} P_{k \times N} \left[x^{(i)} \right] \right] A^{(i-1)} \\ &\quad - P_{N \times k} \left[x^{(i)} \right] D^{(i)} P_{k \times N} \left[x^{(i)} \right] \end{aligned} \quad (21)$$

where $\left[x^{(i)} \right]$ represents the set of positions x_1, x_2, \dots, x_k of k lattice points where the auxiliary field changed during the i -th update of the Green's function. $P_{k \times N} \left[x^{(i)} \right]$ is an index matrix labeling the changed auxiliary fields with k rows and N columns, and has the following form.

$$P_{k \times N} \left[x^{(i)} \right] = [e_{x_1} | e_{x_2} | \cdots | e_{x_k}]^T \quad (22)$$

Additionally, $P_{N \times k} \left[x^{(i)} \right]$ is the transpose matrix of $P_{k \times N} \left[x^{(i)} \right]$.

$$P_{N \times k} \left[x^{(i)} \right] = \left(P_{k \times N} \left[x^{(i)} \right] \right)^T \quad (23)$$

By repeatedly applying the recursive Eq. (21), one can obtain

$$A^{(i)} = \tilde{A}^{(i)} - X^{(i)} Y^{(i)} \quad (24)$$

where $\tilde{A}^{(i)} = (I + X^{(i)} Y^{(i)}) A^{(0)}$ with

$$X^{(i)} = P_{N \times ik} \left[x^{(1)}, \dots, x^{(i)} \right] \begin{pmatrix} D^{(1)} & & \\ & \ddots & \\ & & D^{(i)} \end{pmatrix} \quad (25)$$

$$Y^{(i)} = P_{ik \times N} \left[x^{(1)}, \dots, x^{(i)} \right] \quad (26)$$

We also define $\tilde{G}^{(i)} \equiv (\tilde{A}^{(i)})^{-1}$. In the simulation, we need $G^{(i)}$ instead of its inverse, and by using the Woodbury matrix identity and Eq. (24), we have

$$\begin{aligned} G^{(i)} &= \left[(\tilde{G}^{(i)})^{-1} - X^{(i)} Y^{(i)} \right]^{-1} \\ &= \tilde{G}^{(i)} + \tilde{G}^{(i)} X^{(i)} \left[I_{ik \times ik} - Y^{(i)} \tilde{G}^{(i)} X^{(i)} \right]^{-1} Y^{(i)} \tilde{G}^{(i)} \end{aligned} \quad (27)$$

After simplification, the Green's function can be expressed in the following form

$$\begin{aligned} G^{(i)} &= \left(G^{(0)} + G^{(0)} P_{N \times ik} \left[x^{(1)}, \dots, x^{(i)} \right] \left(\Gamma_{ik \times ik}^{(i)} \right)^{-1} \right. \\ &\quad \left. P_{ik \times N} \left[x^{(1)}, \dots, x^{(i)} \right] G^{(0)} \right) \left(E_{N \times N}^{(i)} \right)^{-1} \end{aligned} \quad (28)$$

This is the key formula of the submatrix update. Here we introduce an $ik \times ik$ matrix $\Gamma_{ik \times ik}^{(i)}$ and a $N \times N$ matrix $(E_{N \times N}^{(i)})^{-1}$. They have the following forms.

$$\Gamma_{ik \times ik}^{(i)} \equiv \begin{pmatrix} I_{k \times k} + (D^{(1)})^{-1} & & \\ & \ddots & \\ & & I_{k \times k} + (D^{(i)})^{-1} \\ -P_{ik \times N} [x^{(1)}, \dots, x^{(i)}] G^{(0)} P_{N \times ik} [x^{(1)}, \dots, x^{(i)}] & & \end{pmatrix} \quad (29)$$

$$(E_{N \times N}^{(i)})^{-1} \equiv \begin{pmatrix} D^{(1)} (I_{k \times k} + D^{(1)})^{-1} & & \\ & \ddots & \\ & & D^{(i)} (I_{k \times k} + D^{(i)})^{-1} \end{pmatrix} P_{ik \times N} [x^{(1)}, \dots, x^{(i)}] \quad (30)$$

After defining the matrix $\Gamma_{ik \times ik}^{(i)}$, we can discuss how to calculate the determinant ratio $\det [S^{(i)}]$ where

$$S^{(i)} = I_{k \times k} + \mathcal{V}^{(i)} D^{(i)} \quad (31)$$

with

$$\mathcal{V}^{(i)} = -P_{k \times N} [x^{(i)}] (G^{(i-1)} - I) P_{N \times k} [x^{(i)}] \quad (32)$$

$$D^{(i)} = \begin{bmatrix} \Delta_{x_1^{(i)} x_1^{(i)}} & 0 & \dots \\ 0 & \Delta_{x_2^{(i)} x_2^{(i)}} & \dots \\ \vdots & \vdots & \ddots \end{bmatrix}_{k \times k} \quad (33)$$

In order to calculate $P_{k \times N} [x^{(i)}] G^{(i-1)} P_{N \times k} [x^{(i)}]$, we can employ Eq. (28). It's evident that every time the acceptance ratio is computed, the inverse of the $\Gamma_{ik \times ik}^{(i)}$ matrix is required. As the number of accepted configurations increases, the dimension of the $\Gamma_{ik \times ik}^{(i)}$ matrix also increases. Recalculating the inverse of the $\Gamma_{ik \times ik}^{(i)}$

matrix after each acceptance would result in a computational complexity of $\mathcal{O}(i^3 k^3)$ for each calculation, which is clearly not a good idea. To mitigate this issue, we use the block matrix inverse formula by rewriting $\Gamma_{ik \times ik}^{(i)}$ matrix (29) in a recursive form.

$$\Gamma_{ik \times ik}^{(i)} = \begin{pmatrix} \Gamma^{(i-1)} & P \\ Q & \Sigma \end{pmatrix} \quad (34)$$

with

$$P = -P_{(i-1)k \times N} [x^{(1)}, \dots, x^{(i-1)}] G^{(0)} P_{N \times k} [x^{(i)}] \quad (35)$$

$$Q = -P_{k \times N} [x^{(i)}] G^{(0)} P_{N \times (i-1)k} [x^{(1)}, \dots, x^{(i-1)}] \quad (36)$$

$$\Sigma = I_{k \times k} + (D^{(i)})^{-1} - P_{k \times N} [x^{(i)}] G^{(0)} P_{N \times k} [x^{(i)}]. \quad (37)$$

Using following block matrix inverse formula,

$$\begin{pmatrix} \Gamma & P \\ Q & \Sigma \end{pmatrix}^{-1} = \begin{pmatrix} \Gamma^{-1} + \Gamma^{-1} P (\Sigma - Q \Gamma^{-1} P)^{-1} Q \Gamma^{-1} & -\Gamma^{-1} P (\Sigma - Q \Gamma^{-1} P)^{-1} \\ -(\Sigma - Q \Gamma^{-1} P)^{-1} Q \Gamma^{-1} & (\Sigma - Q \Gamma^{-1} P)^{-1} \end{pmatrix} \quad (38)$$

we can calculate the inverse of $\Gamma_{ik \times ik}^{(i)}$ matrix with computation complexity $\mathcal{O}(i^2 k^2)$. In order to help readers better understand how to use submatrix updates for local updates, we have created a flowchart illustrating the submatrix update process in Fig. 2.

Here, we offer a brief discussion on the computational

complexity associated with submatrix update. The additional overhead for preparing the intermediate matrices primarily arises from computing $(\Gamma^{(i)})^{-1}$ instead of part of the Green's function in the delay update. Consequently, submatrix update reduces the computational complexity for the additional overhead from $\mathcal{O}(n_d^2 N)$ to

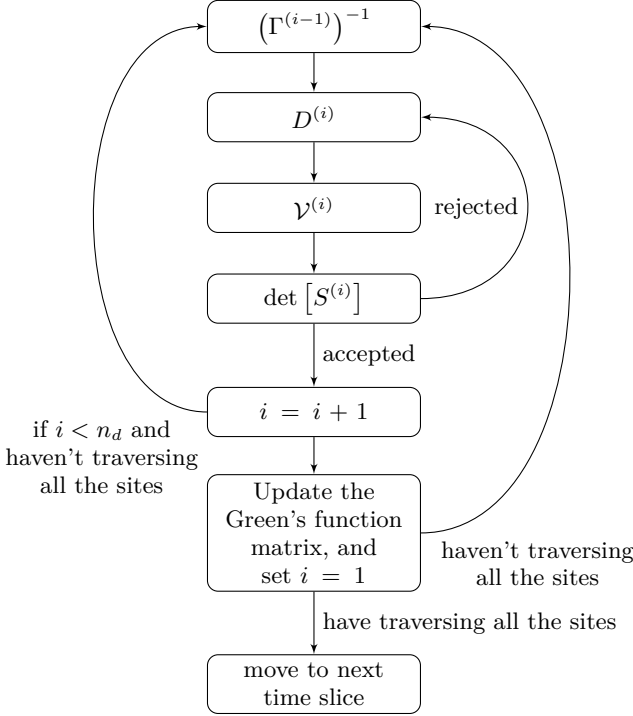


FIG. 2. A flowchart of the submatrix update.

$\mathcal{O}(n_d^3)$ per step of entire Green's function update. In each sweep, we perform a number of entire Green's function updates on the order of $\mathcal{O}(\beta N/n_d)$. This adjustment reduces the computational complexity of the additional overhead from $\mathcal{O}(\beta n_d N^2)$ in the delay update to $\mathcal{O}(\beta n_d^2 N)$ in the submatrix update. However, this reduction comes with a trade-off. In updating the Green's function, additional computations are necessary, that is $(\Gamma_{ik \times ik}^{(i)})^{-1} P_{ik \times N} [x^{(1)}, \dots, x^{(i)}] G^{(0)}$, which has complexity $\mathcal{O}(n_d^2 N)$. Fortunately, this can be done by Level 3 BLAS. Considering the factor of $\mathcal{O}(\beta N/n_d)$ number of entire Green's function update per sweep, this additional calculation has complexity $\mathcal{O}(\beta n_d N^2)$.

To facilitate readers in comparing the computational complexity and the corresponding types of computations between different updating methods, we summarize the results in Table I. Clearly, compared to the delay update, submatrix update reduces the number of Level 1 BLAS calculations, with a trade-off to have more Level 3 BLAS computations which has higher efficiency.

Furthermore, we note that the optimized value of n_d is limited by the size of the cache. Based on ref. [64] and our tests on various platforms, setting kn_d to 2^λ , where $\lambda = \min[6, \lceil \log_2 \frac{N}{12} \rceil]$, has proven to be a good choice. For example, for $N = 60^2$, n_d can be set to 256. The above discussion is based on the finite temperature DQMC, and the zero-temperature version is presented in the Appendix D.

III. MODEL AND RESULTS

To contrast the computational efficiency and the optimization capability in multi-threaded computations of the submatrix update algorithm and the delayed update algorithm, let's first consider onsite interactions ($k = 1$). Note that a case with extended interaction ($k = 2$) is also considered in Appendix C. We first consider the Hubbard model on a square lattice.

$$H_{tU} = -t \sum_{\langle i,j \rangle, \alpha} (c_{i,\alpha}^\dagger c_{j,\alpha} + \text{H.c.}) + \frac{U}{2} \sum_i (n_i - 1)^2 \quad (39)$$

where $c_{i,\alpha}^\dagger$ represents the creation operator for an electron on site i with spin polarization $\alpha = \uparrow / \downarrow$. The operator $n_i = \sum_\alpha c_{i\alpha}^\dagger c_{i\alpha}$ denotes the fermion number density on site i . The parameter t describes the hopping of electrons between NN sites i and j , while U represents the amplitude of the onsite Hubbard repulsive interaction. We set $t = 1$ as the unit of energy and focus on the half-filling case to avoid the sign problem.

After the Hubbard-Stratonovich (HS) transformation, the spin up and down sectors are block diagonalized, allowing for separate calculations of the Green's function for each spin polarization. This is why the Hubbard model serves as an example of the $k = 1$ case for local updates. When $U/t = 0$, the model at half-filling exhibits a diamond-shaped Fermi surface. However, turning on U/t triggers a metal-insulator transition to an antiferromagnetic insulator phase.

To maintain controlled variables, we set the Hubbard repulsive interaction $U/t = 1$, the size of the system $L = 60$, the inverse temperature $\beta t = 1$, and the time slice for Trotter decomposition $\Delta_\tau t = 0.1$, ensuring consistent initial conditions for both algorithms. Each simulation comprises 8 Markov chains, with each chain undergoing 25 sweeps. Let's consider finite-temperature calculations. We record the average computation time for updates per sweep using different local update algorithms for comparison. To study the computational complexity of both algorithms at different n_d , we recorded the computation time for delayed update and submatrix update at various n_d . For ease of comparison, we divided the computation time into two parts: one for computing the acceptance ratio and intermediate matrices, defined as 'ratio,' and the other for updating the Green's function matrix, defined as 'G.' Additionally, we recorded the total time used for the updating process, defined as 'total.' The results are shown in Fig. 3(a).

From the results, it is clear that the time taken to compute the acceptance ratio in submatrix update is significantly less than that in delay update. However, the time taken to update the Green's function matrix is slightly longer in submatrix update compared to delay update, which is consistent with the earlier analysis of their computational complexity. Regardless of whether it's delay update or submatrix update, as n_d increases, the time

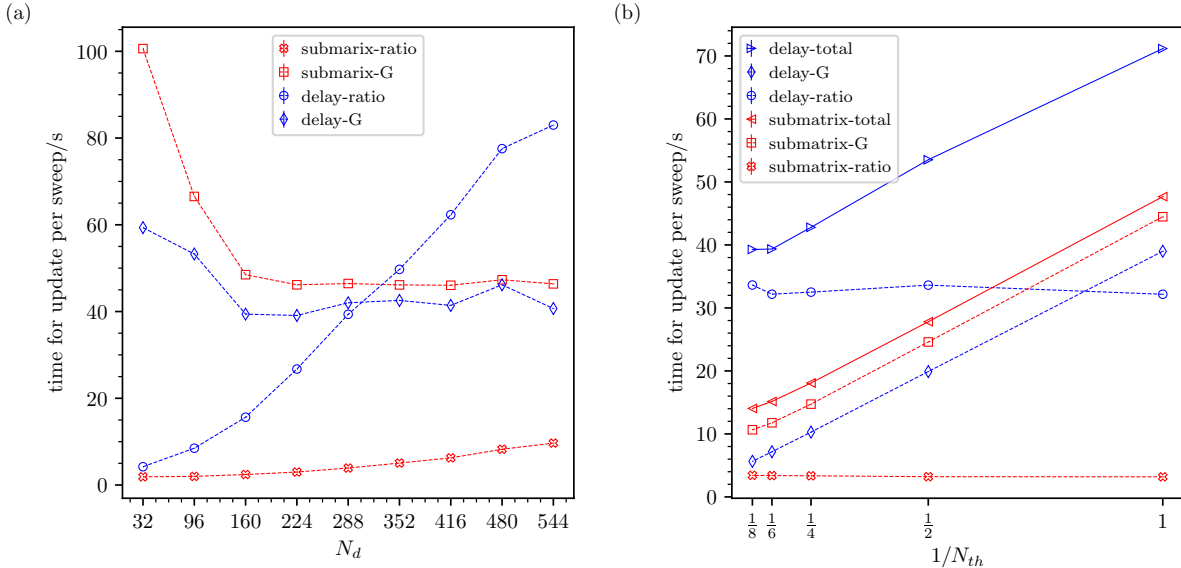


FIG. 3. (a) The time for update per sweep taken by delay update and submatrix update in DQMC-finite-T to compute the acceptance ratio (-ratio) and update the Green's function matrix (-G) of the Hubbard model on a square lattice at different n_d when the number of threads N_{th} is 1. (b) The time for update per sweep taken by delay update and submatrix update in DQMC-finite-T to compute the acceptance ratio (-ratio), update the Green's function matrix (-G) and the total update time (-total) of the Hubbard model on a square lattice at different N_{th} when $n_d = 256$.

taken to compute the acceptance ratio increases accordingly, while the time taken to update the Green's function decreases and eventually converges. Therefore, both methods have an optimal n_d , as mentioned earlier.

To investigate the optimization of different computational components during updating by multiple threads, we fixed n_d for both algorithms to 256 and varied the number of threads N_{th} as 1, 2, 4, 6 and 8. We recorded the time taken for each component under different number of threads. The results are shown in the Fig. 3(b). When the number of threads increases, the time taken to compute the acceptance ratio remains almost constant, or even slightly increases. This is because the ratio calculation part is fragmented and cannot be efficiently paralleled. However, when updating the Green's function matrix, which use Level 3 BLAS and can be effectively paralleled.

It is also interesting to point out that the speedup of multiple threads running is limited by n_d , as we increase the number of threads, the speedup has a tendency to saturate. To verify this effect, we perform tests on different n_d and different numbers of threads N_{th} , and summarize the results in the Fig. 4. It is obvious that as n_d increases, the part of updating the Green's function matrix can utilize threads more efficiently. However, the increase in n_d leads to an increase in the time taken for computing the acceptance ratio, which cannot be accelerated by multiple threads. Therefore, it is necessary to choose an appropriate n_d to maximize the speedup. Similar test for delay update will be discussed in the Appendix B. According to the previous discussion and Ref. [62], submatrix update

has a larger optimal n_d and less Level 1 BLAS calculations than delay update. Therefore, submatrix update is not only more efficient in single-thread running, but is also more suitable for multi-threaded computations. This is crucial for using large-scale parallel computations.

To further demonstrate the capability of submatrix update, we utilize this method to compute the phase diagram of the Néel transition in the half-filled Hubbard model on a 3D cubic lattice. In the literatures, only system sizes up to 1000 lattice sites ($N = 1000$) [10], are available. We show that with the help of submatrix update, it becomes feasible to compute much larger system sizes for the 3D Hubbard model.

When the 3D Hubbard model enters the antiferromagnetic phase, it develops long range spin correlations. The Fourier transform of the spin correlation function defines the spin structure factor, which has following form,

$$S(\mathbf{q}) \equiv \frac{1}{N^2} \sum_{i,j} e^{i\mathbf{q} \cdot (\mathbf{r}_i - \mathbf{r}_j)} \langle \vec{S}_i \cdot \vec{S}_j \rangle \quad (40)$$

The $\mathbf{q} = \mathbf{Q} \equiv (\pi, \pi, \pi)$ structure factor $S(\mathbf{Q})$ is related to the magnetization m . In the thermodynamic limit (TDL), $\lim_{L \rightarrow \infty} S(\mathbf{Q}) = m^2$. To study the AFM phase transition, we introduce a correlation ratio, which is a dimensionless quantity with following form:

$$r_S \equiv 1 - \frac{S(\mathbf{Q} + d\mathbf{q})}{S(\mathbf{Q})}, \quad (41)$$

where $d\mathbf{q} = (\frac{2\pi}{L}, 0, 0)$. The correlation ratio can be used to identify the critical point of the phase transition. As

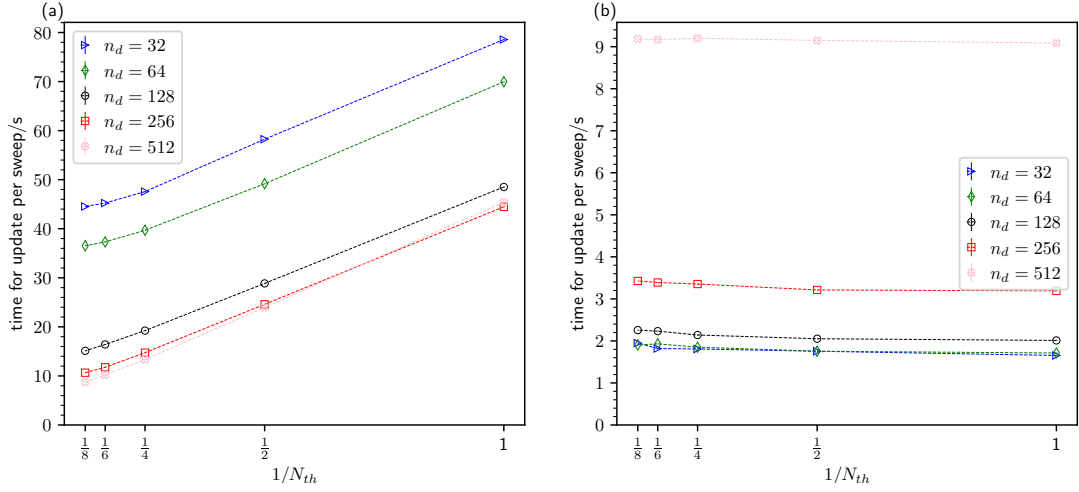


FIG. 4. (a) The relationship between the time for update per sweep taken to update the Green's function matrix in submatrix update and the number of threads N_{th} for different n_d values in DQMC-finite-T of the Hubbard model on a square lattice $L = 60$. (b) The relationship between the time for update per sweep taken to calculate in submatrix update and the number of threads N_{th} for different n_d values in DQMC-finite-T of the Hubbard model on a square lattice $L = 60$.

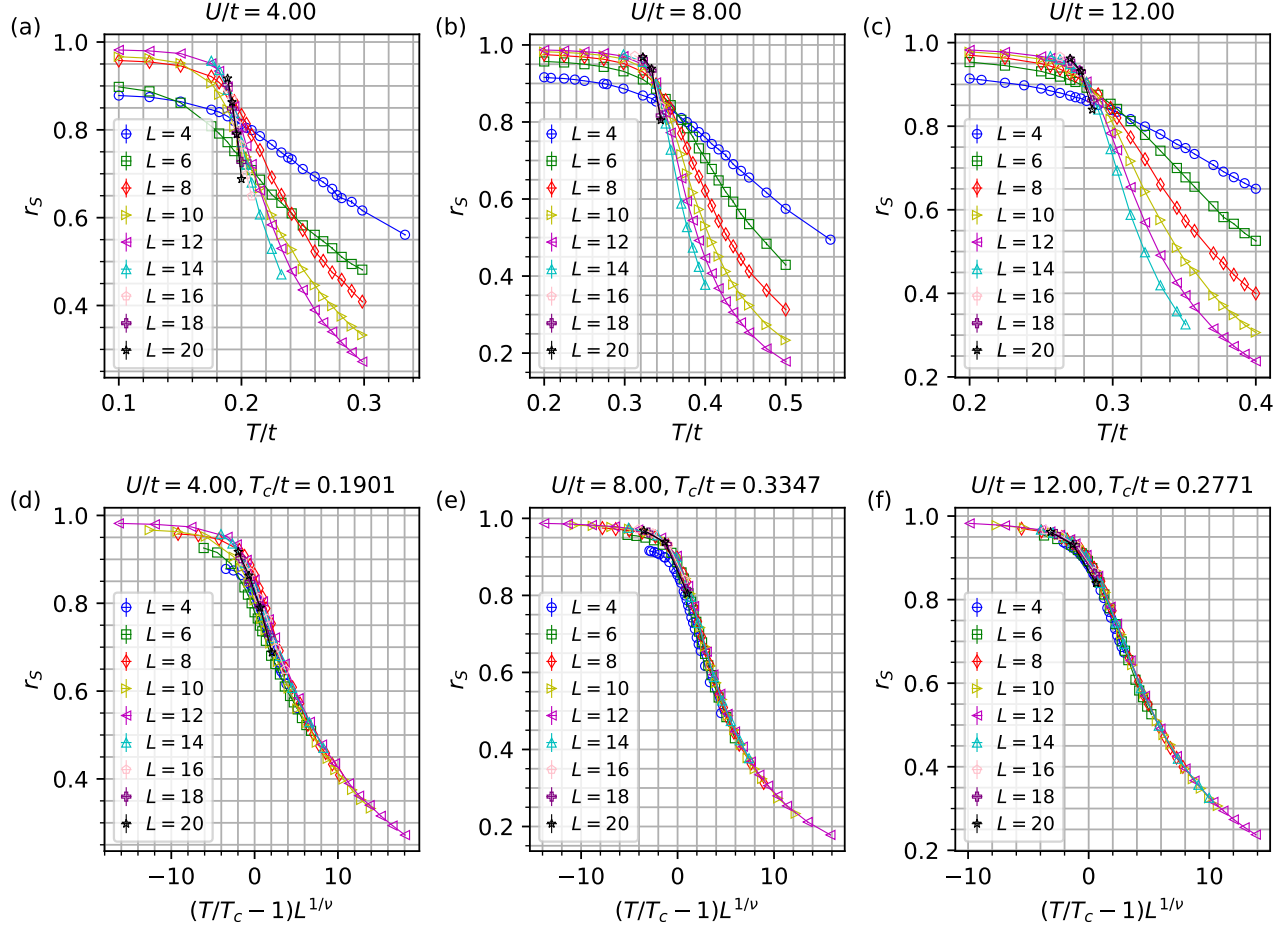


FIG. 5. (a), (b) and (c), scanning of r_S at different temperatures for $U/t = 4.00, 8.00, 12.00$ to obtain the critical temperatures T_c . (d), (e) and (f), the data collapse of the r_S for $U/t = 4.00, 8.00, 12.00$, where $\nu = 0.707$.

the finite temperature AFM transition is known to be a $O(3)$ transition, its critical exponents are well known, which can be used to double check our calculations. The correlation ratio as a dimensionless quantity has following scaling behavior

$$r_S(T, L) = f \left(\frac{T - T_c}{T_c} L^{\frac{1}{\nu}} \right) \quad (42)$$

where $\nu \approx 0.707$. At the transition temperature T_c , the $r_S - T$ curves for different L intersect. We consider $U/t = 4, 6, 8, 10, 12$ and perform scans of r_S of the 3D Hubbard model on a cubic lattice ($N = L^3$) at different temperatures using submatrix update for various L values (up to $L = 20$) to get the critical temperature T_c . The results are shown in Fig. 5 and 7.

From the computational results, as mentioned earlier, below the Néel temperature, the system enters the AFM state, where the spin correlation function $S(\mathbf{Q})$ tends to diverge. This results in r_s increasing from 0 to 1 after entering the AFM state. According to previous analysis, r_s for different sizes eventually intersect at a single point, and the abscissa of this point corresponds to the critical temperature at the Néel phase transition. However, the actual results may deviate from this prediction due to finite-size effects. To ensure the reliability of the results, we need to analyze the finite-size effects and extrapolate them to the TDL. We search for the intersections of r_s between adjacent sizes (L and $L + 2$), extract these intersection points, and extrapolate them to $L \rightarrow \infty$ using function $T = aL^{-b} + T_c$ to find the critical temperature in the TDL. The results are shown in Fig. 6. From the

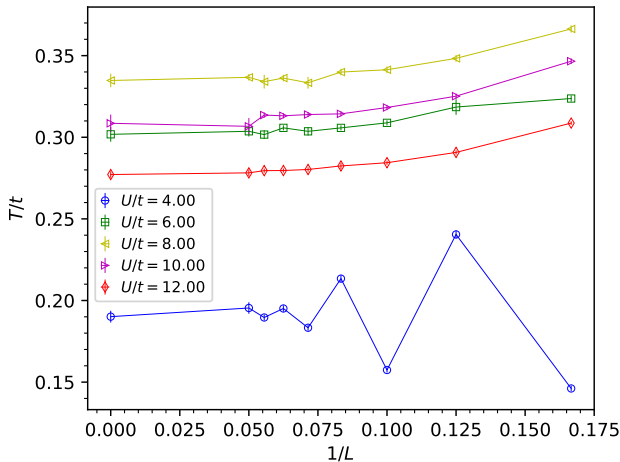


FIG. 6. The finite-size effects for different U/t values are analyzed using correlation ratio crossing. The uncertainty is estimated by moving the intersection segment within the error bars of r_S between adjacent sizes (L and $L + 2$). The error bar for the critical temperature T_c is estimated through error propagation of the errors at each point.

results, we successfully obtained the Néel transition temperatures in the thermodynamic limit using this method

for $U/t = 6, 8, 10$ and 12 . However, for $U/t = 4$, the intersection points fluctuate, making it difficult to extrapolate using adjacent points. This is due to the stronger finite-size effects when U is small. Therefore, we divided the points into two groups using next adjacent size (L and $L + 4$), and utilize the function $T = aL^{-b} + T_c$ for separate extrapolation for each group. The critical transition temperatures obtained by extrapolating these two sets of data are 0.1901 ± 0.0036 and 0.1892 ± 0.0029 . We found that both results fall within the error bar. Ultimately, we chose the one with the larger error as the final value for the critical transition temperature at $U/t = 4$. The final result for the critical Néel transition temperature of the 3D half-filled Hubbard model is shown in Table III.

TABLE II. The Néel temperature of the 3D half-filled Hubbard model on a cubic lattice.

U/t	T_c/t
4	0.1901(36)
6	0.3017(45)
8	0.3347(42)
10	0.3085(54)
12	0.2771(20)

We utilize this data to plot the phase diagram of the Néel transition for the 3D half-filled Hubbard model on a cubic lattice, as shown in Fig. 1(b).

Finally, we validate the accuracy of the critical transition temperatures obtained for different interaction strengths. According to the description of formula Eqs. (42) earlier, when the correct critical temperature is obtained, data from all different sizes will collapse onto a single curve. The final result is shown in Fig. 5 and 7.

It shows that when U/t is relatively small, the finite-size effects from small sizes do not result in a good collapse onto a single curve. However, as the size or U/t increases, the influence of finite-size effects decreases significantly, eventually allowing the data to collapse onto a single curve. This also indicates the necessity of computing large-size models to obtain more accurate results.

IV. CONCLUSION AND DISCUSSION

In this work, we have developed a general submatrix update method to further optimize the computational efficiency of DQMC. This method is applicable to both onsite and extended interactions and demonstrates optimization capabilities under both zero-temperature and finite-temperature conditions. In our tests, the submatrix update method not only exhibits higher computational efficiency compared to delayed updating for single thread running, but also offers better optimization in multi-threaded computations, which is more suitable for large size calculations. Subsequently, we utilized this method to compute the phase diagram of the Néel transition for the three-dimensional half-filled Hubbard model on a cubic lattice. By computing system size up to 8,000

sites, we obtained more accurate phase diagram of 3D Hubbard model at half-filling. This result will be useful for guiding the cold atom simulation of 3D Hubbard model [66].

Looking forward, our submatrix update is general, and can be used to accelerate the simulation of 2D Dirac fermions with interactions. By pushing the simulation of the system size to the order of 100^2 , we foresee that we will have converging results for the critical exponents of Gross-Neveu transitions in many interacting Dirac fermion systems. At the same time, it will help to distinguish from weakly first order to a continuous transition in the situations when the finite size effect is very large. It will bring more insights into possible deconfined quantum criticality in fermionic systems, as well as shed light on critical Fermi surface problem where simulating larger system size is essential.

ACKNOWLEDGMENTS

Acknowledgments— X.Y.X. is sponsored by the National Natural Science Foundation of China (Grants No. 12274289), the National Key R&D Program of China (Grant No. 2022YFA1402702, No. 2021YFA1401400), the Innovation Program for Quantum Science and Technology (under Grant no. 2021ZD0301900), Yangyang Development Fund, and startup funds from SJTU.

Appendix A: Other data for 3D Hubbard model

The correlation ratio and its data collapse for $U/t = 6$ and $U/t = 10$ are presented in Fig. 7.

Appendix B: Delay update under multi-threads

To compare with the submatrix update results under multi-threads as shown in Fig. 4, we also perform similar test for delay update. We set n_d for delay update to 32, 64, 128, 256 and 512, and consider different numbers of threads N_{th} . We record the time taken for each component, and the results are similar to submatrix update as shown in the Fig. 8. The Green's function update part shows nearly perfect speedup under multi-threads running, while the ratio calculation part does not show any significant speedup. Therefore reduce the time cost for the ratio calculation part is essential to improve the efficiency, and that is exactly what submatrix update algorithm does.

Appendix C: The submatrix update of DQMC-finite-T in spinless t-V model

We have demonstrated the optimization achieved by submatrix update in the presence of onsite interaction

($k = 1$). Now, let's explore its optimization in extended interaction. We consider a model where Δ contains only two non-zero diagonal elements ($k = 2$). The t - V model serves as a such kind of example. It is a spinless fermion model with NN interaction. Let's consider this model on a square lattice. The Hamiltonian is written as

$$H_{tV} = -t \sum_{\langle i,j \rangle} (c_i^\dagger c_j + \text{H.c.}) + V \sum_{\langle i,j \rangle} (n_i - \frac{1}{2})(n_j - \frac{1}{2}) \quad (\text{C1})$$

In the model, c_i^\dagger represents the fermionic creation operator on site i , t denotes the NN hopping amplitude, and $V > 0$ signifies the density repulsive interaction between NN sites. We maintain $t = 1$ as the unit of energy and concentrate on the half-filling case, which still allows for a suitable Hubbard-Stratonovich transformation to circumvent the sign problem [32, 33]. However, this transformation leads to two non-zero off-diagonal elements in Δ during updates. To enable the use of submatrix updates, we require Δ to have only non-zero diagonal elements. We achieve this by diagonalizing $e^{V(\mathbf{s}_i, l)}$ and propagating the Green's function to obtain a representation where Δ is diagonal and contains only two non-zero diagonal elements.

In the simulation, we set $V/t = 1$, and keep all other conditions identical to those of the Hubbard model discussed earlier. Subsequently, we separately employed delay update and submatrix update to conduct DQMC-finite-T calculations on the spinless t - V model. We then compared the performance of these two update methods. It exhibits almost similar phenomena as the Hubbard model, as shown in Fig. 9.

Appendix D: The submatrix update in the zero-temperature version of DQMC

TABLE III. The computational complexity and types of computations required for various local updates in DQMC-zero-T.

	fast update	delay update	submatrix update
Intermediate matrices	-	$\mathcal{O}(\beta n_d N^2)$	$\mathcal{O}(\beta n_d^2 N)$
		Level 1	Level 1
update- G	$\mathcal{O}(\beta N_p^2 N)$	$\mathcal{O}(\beta N^3)$	$\mathcal{O}(\beta N^3 + \beta n_d N^2)$
	Level 1	Level 3	Level 3

The aforementioned submatrix update scheme can also be applied to the zero-temperature version of DQMC. In the zero-temperature version of DQMC (DQMC-zero-T), the normalization factor of the ground state wavefunction $|\Psi_0\rangle$ plays a role similar to the partition function in the finite-temperature case. We perform the HS transformation on the interaction part and trace out the fermions' degree of freedom in the Fock space with a fixed number of particles N_p . Then, we have:

$$\langle \Psi_0 | \Psi_0 \rangle = \sum_s \det [P^\dagger B_s(2\Theta, 0) P] \quad (\text{D1})$$

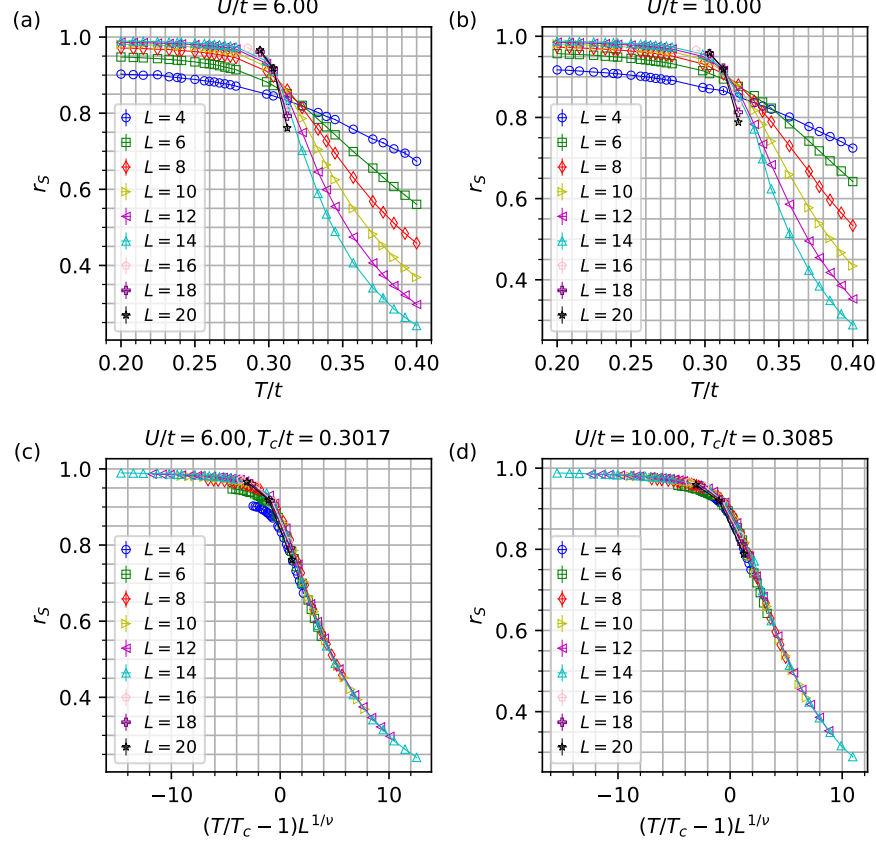


FIG. 7. (a) and (b), scanning of r_S at different temperatures for $U/t = 6.00, 10.00$ to obtain the critical temperatures T_c . (c) and (d), the data collapse of the r_S for $U/t = 6.00, 10.00$, where $\nu = 0.707$.

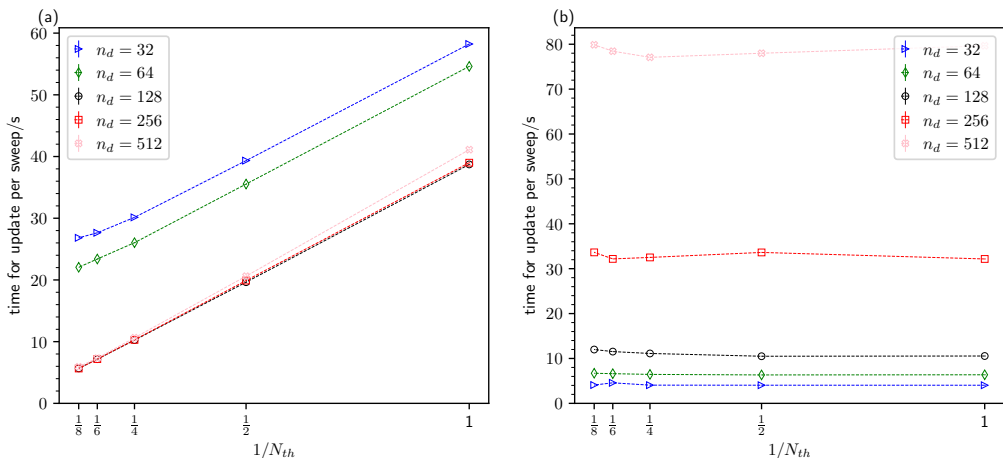


FIG. 8. (a) The relationship between the time for update per sweep taken to update the Green's function matrix in delay update and the number of threads N_{th} for different n_d values in DQMC-finite-T of the Hubbard model on a square lattice $L = 60$. (b) The relationship between the time for update per sweep taken to calculate in delay update and the number of threads N_{th} for different n_d values in DQMC-finite-T of the Hubbard model on a square lattice $L = 60$.

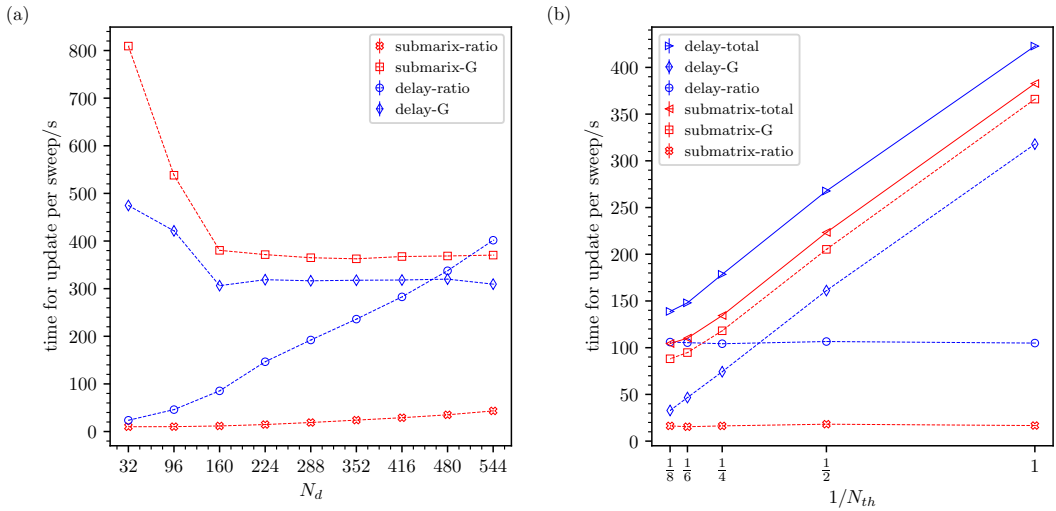


FIG. 9. (a) The time for update per sweep taken by delay update and submatrix update in DQMC-finite-T to compute the acceptance ratio (-ratio) and update the Green's function matrix (-G) of the t - V model on a square lattice at different n_d when the number of threads N_{th} is 1. (b) The time for update per sweep taken by delay update and submatrix update in DQMC-finite-T to compute the acceptance ratio (-ratio), update the Green's function matrix (-G) and the total update time (-total) of the t - V model on a square lattice at different N_{th} when $n_d = 256$.

where we have represent the ground state wavefunction as a projection of a certain trial wavefunction, that is $|\Psi_0\rangle = e^{-\Theta H}|\Psi_T\rangle$, where Θ is the projection time and needs to be sufficiently large to project to the ground state. The trial wavefunction can be represented as a Slater determinant $|\Psi_T\rangle = \prod_{i=1}^{N_p} (\mathbf{c}^\dagger P)_i |0\rangle$, where $|0\rangle$ is a vacuum state, N_p is the number of particles in the ground state, and P is a matrix with dimensions $N \times N_p$. Typically, we choose the trial wavefunction to be the ground state of the non-interacting part $H_0 = \mathbf{c}^\dagger K \mathbf{c}$, and then P consists of N_p lowest eigenvectors of K . For consistency, we will interchangeably use 2Θ and β when necessary.

In the zero-temperature case, we define $B^\langle(\tau) \equiv B(\tau, 0)P$ and $B^\langle(\tau) \equiv P^\dagger B(2\Theta, \tau)$. For the simplification, we will omit τ dependence of B^\langle and B^\rangle in the following discussion by default. In DQMC-zero-T, during

the fast update, we keep track of B^\langle , B^\rangle , and $(B^\langle B^\rangle)^{-1}$ instead of the Green's function. After each local update, B^\rangle is updated to $(I + \Delta)B^\rangle$, and the formula to calculate the determinant ratio is identical to the finite temperature case as shown in Eq. (9). The only extra calculation is that the Green's function elements in \mathcal{V} as shown in Eq. (11) should be calculated explicitly. Note that $G(\tau, \tau) = I - B^\langle (B^\langle B^\rangle)^{-1} B^\rangle$ in DQMC-zero-T, so the calculation Green function elements for calculating ratio has complexity $\mathcal{O}(\beta N N_p^2)$ per sweep. If the update is accepted, we update B^\rangle and $(B^\langle B^\rangle)^{-1}$, and the computational complexity is also $\mathcal{O}(\beta N N_p^2)$ per sweep. According to the previous derivation, we can apply the submatrix update to the zero-temperature case by working with $F^{(i)}$ instead of working with B^\langle , B^\rangle , and $(B^\langle B^\rangle)^{-1}$. In zero-temperature DQMC, $F^{(i)}$ can be defined as:

$$\begin{aligned} F^{(i)} &\equiv (B^\rangle)^{(0)} \left((B^\langle)^{(i)} (B^\rangle)^{(i)} \right)^{-1} (B^\rangle)^{(0)} \\ &= F^{(0)} - F^{(0)} P_{N \times ik} [x^{(1)}, \dots, x^{(i)}] \left(\Gamma_{ik \times ik}^{(i)} \right)^{-1} P_{ik \times N} [x^{(1)}, \dots, x^{(i)}] F^{(0)} \end{aligned} \quad (\text{D2})$$

and

$$F^{(0)} = (B^\rangle)^{(0)} \left((B^\langle)^{(0)} (B^\rangle)^{(0)} \right)^{-1} (B^\langle)^{(0)}. \quad (\text{D3})$$

We have utilized

$$(B^\langle(\tau))^{(i)} = (I + X^{(i)} Y^{(i)}) (B^\langle(\tau))^{(0)} \quad (\text{D4})$$

$$(B^\langle(\tau))^{(i)} = (B^\langle(\tau))^{(0)} \quad (\text{D5})$$

where $X^{(i)}$ and $Y^{(i)}$ are defined in Eq. (25) and Eq. (26). Also note that following relations

$$P_{k \times N} [x^{(i+1)}] (B^\langle(\tau))^{(i)} = P_{k \times N} [x^{(i+1)}] (B^\langle(\tau))^{(0)} \quad (\text{D6})$$

$$(B^\langle(\tau))^{(i)} P_{N \times k} [x^{(i+1)}] = (B^\langle(\tau))^{(0)} P_{N \times k} [x^{(i+1)}] \quad (\text{D7})$$

are useful for obtaining Green's function elements for the determinant ratio calculation in particularly constructing \mathcal{V} defined in Eq. (11). For example, in the i -th step, $\mathcal{V}^{(i)}$ can be calculated by

$$\begin{aligned} \mathcal{V}^{(i)} &= P_{k \times N} [x^{(i)}] (I - G^{(i-1)}) P_{N \times k} [x^{(i)}] \\ &= P_{k \times N} [x^{(i)}] F^{(i-1)} P_{N \times k} [x^{(i)}] \end{aligned} \quad (\text{D8})$$

In the real calculation, $F^{(i)}$ is not calculated at any step, instead, we keep track of $(\Gamma^{(i)})^{-1}$ as in the submatrix

update for DQMC-finite-T. One can see, the submatrix update formula for zero-temperature case is quite similar to finite-temperature case with only a little difference. At the beginning of local update in each time slice, we have to calculate $F^{(0)}$ using Eq. (D3) which has computational complexity $\mathcal{O}(N_p^2 N + N_p^3)$ in each time slice, and we have β time slices, therefore the computational complexity is $\mathcal{O}(\beta N_p^2 N + \beta N_p^3)$ per sweep. Note that computational complexity of submatrix update based on $F^{(i)}$ is $\mathcal{O}(\beta N^3 + \beta n_d N^2)$, similar to the DQMC-finite-T case. As $N_p < N$, the computational complexity for the Green's function update in total is still $\mathcal{O}(\beta N^3 + \beta n_d N^2)$ in submatrix update. Since the calculation is dominant by the calculation with complexity $\mathcal{O}(\beta N^3)$, the time taken for updating the Green's function matrix in DQMC-zero-T is almost the same for both delay update and submatrix update, as shown in Fig. 10 for Hubbard model and Fig. 11 for t - V model.

Appendix E: The choose of the Δ_τ

Due to the mentioned system errors introduced by Trotter decomposition, we need to ensure that extrapolating the phase transition point is not affected by errors. This requires $\Delta_\tau \rightarrow 0$. However, when Δ_τ is small, it leads to numerous time slices, consuming significant computational resources. Hence, we need to find an appropriate Δ_τ . To determine the suitable Δ_τ , we conducted a test before the computation. As Δ_τ decreases, r_S continuously decreases, and eventually converges at

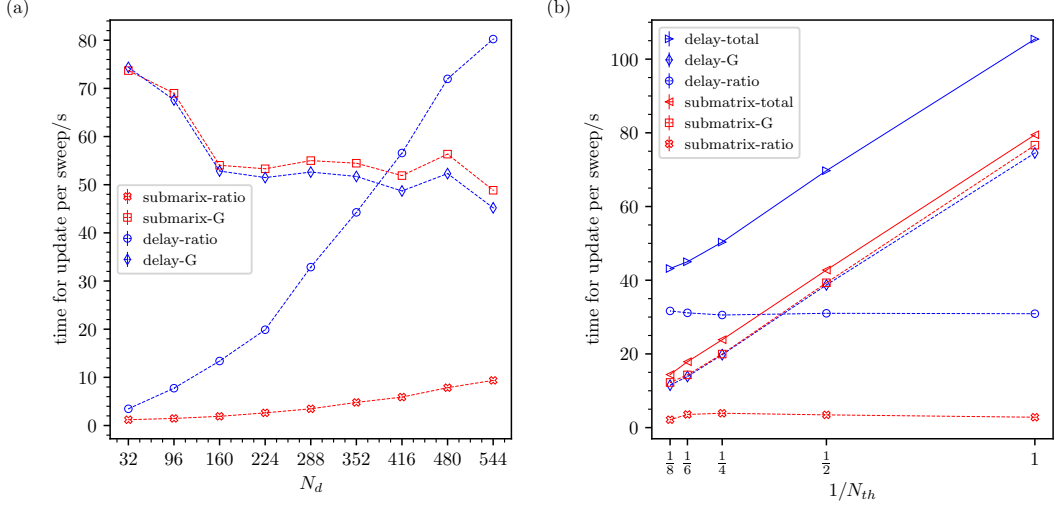


FIG. 10. (a) The time for update per sweep taken by delay update and submatrix update in DQMC-zero-T to compute the acceptance ratio (-ratio) and update the Green's function matrix (-G) of the Hubbard model on a square lattice at different n_d when the number of threads N_{th} is 1. (b) The time for update per sweep taken by delay update and submatrix update in DQMC-zero-T to compute the acceptance ratio (-ratio), update the Green's function matrix (-G) and the total update time (-total) of the Hubbard model on a square lattice at different N_{th} when $n_d = 256$.

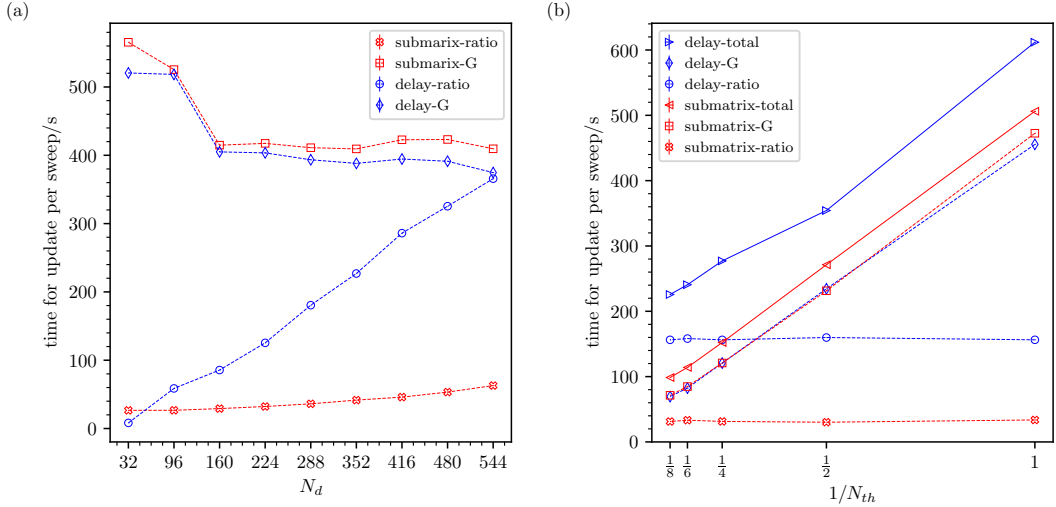


FIG. 11. (a) The time for update per sweep taken by delay update and submatrix update in DQMC-zero-T to compute the acceptance ratio (-ratio) and update the Green's function matrix (-G) of the t - V model on a square lattice at different n_d when the number of threads N_{th} is 1. (b) The time for update per sweep taken by delay update and submatrix update in DQMC-zero-T to compute the acceptance ratio (-ratio), update the Green's function matrix (-G) and the total update time (-total) of the t - V model on a square lattice at different N_{th} when $n_d = 256$.

$\Delta_\tau t = 0.05$ as shown in Fig. 12. Therefore, for computing the phase diagram, we set $\Delta_\tau t$ to 0.05.

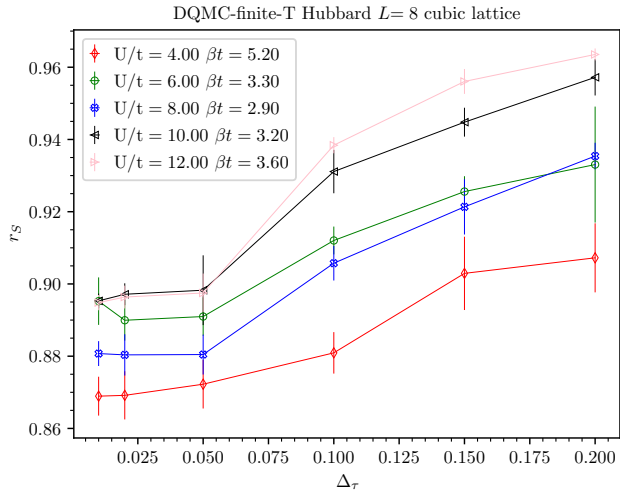


FIG. 12. The relationship between r_S and Δ_τ in DQMC-finite-T of the Hubbard model on a cubic lattice when $L = 8$.

[1] E. Dagotto, International Journal of Modern Physics B **05**, 77 (1991), <https://doi.org/10.1142/S0217979291000067>.

[2] S. R. White, Phys. Rev. Lett. **69**, 2863 (1992).

[3] U. Schollwöck, Rev. Mod. Phys. **77**, 259 (2005).

[4] A. Georges, G. Kotliar, W. Krauth, and M. J. Rozenberg, Rev. Mod. Phys. **68**, 13 (1996).

[5] E. Kozik, M. Ferrero, and A. Georges, Phys. Rev. Lett. **114**, 156402 (2015).

[6] O. Gunnarsson, G. Rohringer, T. Schäfer, G. Sangiovanni, and A. Toschi, Phys. Rev. Lett. **119**, 056402 (2017).

[7] J. E. Hirsch, Phys. Rev. B **35**, 1851 (1987).

[8] E. Kozik, E. Burovski, V. W. Scarola, and M. Troyer, Phys. Rev. B **87**, 205102 (2013).

[9] P. R. C. Kent, M. Jarrell, T. A. Maier, and T. Pruschke, Phys. Rev. B **72**, 060411 (2005).

[10] R. Staudt, M. Dzierzawa, and A. Muramatsu, The European Physical Journal B - Condensed Matter and Complex Systems **17**, 411 (2000).

[11] G. Rohringer, A. Toschi, A. Katanin, and K. Held, Phys. Rev. Lett. **107**, 256402 (2011).

[12] D. Hirschmeier, H. Hafermann, E. Gull, A. I. Lichtenstein, and A. E. Antipov, Phys. Rev. B **92**, 144409 (2015).

[13] R. Blankenbecler, D. J. Scalapino, and R. L. Sugar, Phys. Rev. D **24**, 2278 (1981).

[14] D. J. Scalapino and R. L. Sugar, Phys. Rev. B **24**, 4295 (1981).

[15] J. E. Hirsch, Phys. Rev. B **28**, 4059 (1983).

[16] G. Sugiyama and S. Koonin, Annals of Physics **168**, 1 (1986).

[17] S. Sorella, E. Tosatti, S. Baroni, R. Car, and M. Parrinello, International Journal of Modern Physics B **02**, 993 (1988).

[18] S. Sorella, S. Baroni, R. Car, and M. Parrinello, Europhysics Letters (EPL) **8**, 663 (1989).

[19] E. Loh Jr and J. Gubernatis, Electronic Phase Transitions **32**, 177 (1992).

[20] S. E. Koonin, D. J. Dean, and K. Langanke, Physics reports **278**, 1 (1997).

[21] F. Assaad and H. Evertz, World-line and determinantal quantum monte carlo methods for spins, phonons and electrons, in *Computational Many-Particle Physics*, edited by H. Fehske, R. Schneider, and A. Weiße (Springer Berlin Heidelberg, Berlin, Heidelberg, 2008) pp. 277–356.

[22] J. E. Hirsch, Phys. Rev. B **31**, 4403 (1985).

[23] S. R. White, D. J. Scalapino, R. L. Sugar, E. Y. Loh, J. E. Gubernatis, and R. T. Scalettar, Phys. Rev. B **40**, 506 (1989).

[24] F. F. Assaad, Phys. Rev. Lett. **83**, 796 (1999).

[25] D. Scalapino, Numerical studies of the 2d hubbard model, in *Handbook of High-Temperature Superconductivity* (Springer, 2007) pp. 495–526.

[26] D. Zheng, G.-M. Zhang, and C. Wu, Phys. Rev. B **84**, 205121 (2011).

[27] M. Hohenadler, T. C. Lang, and F. F. Assaad, Phys. Rev. Lett. **106**, 100403 (2011).

[28] E. Berg, M. A. Metlitski, and S. Sachdev, Science **338**, 1606 (2012).

[29] M. Hohenadler and F. F. Assaad, Journal of Physics: Condensed Matter **25**, 143201 (2013).

[30] F. F. Assaad and I. F. Herbut, Phys. Rev. X **3**, 031010 (2013).

[31] J. P. F. LeBlanc, A. E. Antipov, F. Becca, I. W. Bulik, G. K.-L. Chan, C.-M. Chung, Y. Deng, M. Ferrero, T. M. Henderson, C. A. Jiménez-Hoyos, E. Kozik, X.-W. Liu, A. J. Millis, N. V. Prokof'ev, M. Qin, G. E. Scuseria, H. Shi, B. V. Svistunov, L. F. Tocchio, I. S. Tupitsyn, S. R. White, S. Zhang, B.-X. Zheng, Z. Zhu, and E. Gull (Simons Collaboration on the Many-Electron Problem), Phys. Rev. X **5**, 041041 (2015).

[32] Z.-X. Li, Y.-F. Jiang, and H. Yao, Phys. Rev. B **91**, 241117 (2015).

[33] L. Wang, Y.-H. Liu, M. Iazzi, M. Troyer, and G. Harcos, Phys. Rev. Lett. **115**, 250601 (2015).

[34] Y.-Y. He, H.-Q. Wu, Y.-Z. You, C. Xu, Z. Y. Meng, and Z.-Y. Lu, Phys. Rev. B **93**, 115150 (2016).

[35] Y. Otsuka, S. Yunoki, and S. Sorella, Phys. Rev. X **6**, 011029 (2016).

[36] F. Assaad and T. Grover, Physical Review X **6**, 041049 (2016).

[37] Z. Zhou, D. Wang, Z. Y. Meng, Y. Wang, and C. Wu, Phys. Rev. B **93**, 245157 (2016).

[38] S. Gazit, M. Randeria, and A. Vishwanath, Nature Physics **13**, 484 (2017).

[39] E. Berg, S. Lederer, Y. Schattner, and S. Trebst, Annual Review of Condensed Matter Physics **10**, 63 (2019).

[40] Z.-X. Li and H. Yao, Annual Review of Condensed Matter Physics **10**, 337 (2019).

[41] X. Y. Xu, Z. H. Liu, G. Pan, Y. Qi, K. Sun, and Z. Y. Meng, Journal of Physics: Condensed Matter **31**, 463001 (2019).

[42] Y. Liu, Z. Wang, T. Sato, M. Hohenadler, C. Wang, W. Guo, and F. F. Assaad, Nature Communications **10**, 2658 (2019).

[43] X. Y. Xu, Y. Qi, L. Zhang, F. F. Assaad, C. Xu, and Z. Y. Meng, Physical Review X **9**, 021022 (2019).

[44] C. Chen, X. Y. Xu, Z. Y. Meng, and M. Hohenadler, Phys. Rev. Lett. **122**, 077601 (2019).

[45] Y.-X. Zhang, W.-T. Chiu, N. C. Costa, G. G. Batrouni, and R. T. Scalettar, Phys. Rev. Lett. **122**, 077602 (2019).

[46] X. Y. Xu and T. Grover, Phys. Rev. Lett. **126**, 217002 (2021).

[47] X. Zhang, G. Pan, Y. Zhang, J. Kang, and Z. Y. Meng, Chinese Physics Letters **38**, 077305 (2021).

[48] J. S. Hofmann, E. Khalaf, A. Vishwanath, E. Berg, and J. Y. Lee, Physical Review X **12**, 011061 (2022).

[49] R. Mondaini, S. Tarat, and R. T. Scalettar, Science **375**, 418 (2022).

[50] J. Ostmeyer, E. Berkowitz, S. Krieg, T. A. Lähde, T. Luu, and C. Urbach, Phys. Rev. B **102**, 245105 (2020).

[51] E. Huffman and S. Chandrasekharan, Phys. Rev. D **101**, 074501 (2020).

[52] S. Beyl, F. Goth, and F. F. Assaad, Phys. Rev. B **97**, 085144 (2018).

[53] R. Brower, C. Rebbi, and D. Schaich, arXiv:1204.5424 (2012).

[54] R. Brower, C. Rebbi, and D. Schaich, arXiv:1204.5424 (2012).

[55] T. Luu and T. A. Lähde, Phys. Rev. B **93**, 155106 (2016).

[56] J.-L. Wynen, E. Berkowitz, C. Körber, T. A. Lähde, and T. Luu, Phys. Rev. B **100**, 075141 (2019).

[57] M. Ulybyshev, S. Zafeiropoulos, C. Winterowd, and F. Assaad, arXiv:2104.09655 (2021).

[58] D. Banerjee and E. Huffman, Phys. Rev. D **109**, L031506 (2024).

[59] J. Liu, Y. Qi, Z. Y. Meng, and L. Fu, Phys. Rev. B **95**, 041101 (2017).

[60] X. Y. Xu, Y. Qi, J. Liu, L. Fu, and Z. Y. Meng, Phys. Rev. B **96**, 041119 (2017).

[61] Y.-Y. He, H. Shi, and S. Zhang, Phys. Rev. Lett. **123**, 136402 (2019).

[62] F. Sun and X. Y. Xu, Delay update in determinant quantum monte carlo (2023), arXiv:2308.12005 [cond-mat.str-el].

[63] G. Alvarez, M. S. Summers, D. E. Maxwell, M. Eisenbach, J. S. Meredith, J. M. Larkin, J. Levesque, T. A. Maier, P. R. Kent, E. F. D'Azevedo, *et al.*, in *SC'08: Proceedings of the 2008 ACM/IEEE Conference on Supercomputing* (IEEE, 2008) pp. 1–10.

[64] P. K. V. V. Nukala, T. A. Maier, M. S. Summers, G. Alvarez, and T. C. Schulthess, Phys. Rev. B **80**, 195111 (2009).

[65] E. Gull, P. Staar, S. Fuchs, P. Nukala, M. S. Summers, T. Pruschke, T. C. Schulthess, and T. Maier, Phys. Rev. B **83**, 075122 (2011).

[66] H.-J. Shao, Y.-X. Wang, D.-Z. Zhu, Y.-S. Zhu, H.-N. Sun, S.-Y. Chen, C. Zhang, Z.-J. Fan, Y. Deng, X.-C. Yao, *et al.*, arXiv:2402.14605 (2024).

[67] Y. Ouyang and X. Y. Xu, Phys. Rev. B **104**, L241104 (2021).

[68] X. Zhang, G. Pan, X. Y. Xu, and Z. Y. Meng, Phys. Rev. B **106**, 035121 (2022).

[69] X. Xu, Acta Phys. Sin **71**, 127101 (2022).

[70] M. C. Gutzwiller, Phys. Rev. Lett. **10**, 159 (1963).

[71] J. Hubbard, Proceedings of the Royal Society of London. Series A. Mathematical and Physical Sciences **276**, 238 (1963).

[72] D. P. Arovas, E. Berg, S. A. Kivelson, and S. Raghu, Annual review of condensed matter physics **13**, 239 (2022).

[73] M. Qin, T. Schäfer, S. Andergassen, P. Corboz, and E. Gull, Annual Review of Condensed Matter Physics **13**, 275 (2022).